Universidade de Aveiro Departamento de Física
2011

Tiago José Águeda Oliveira

Modelação *Ab Initio* de Defeitos Pontuais de Boro em Silício Amorfo

Ab Initio Modeling of Boron Related Point Defects in Amorphous Silicon

Universidade de Aveiro Departamento de Física
2011

Tiago José Águeda Oliveira

Modelação *Ab Initio* de Defeitos Pontuais de Boro em Silício Amorfo

Ab Initio Modeling of Boron Related Point Defects in Amorphous Silicon

Dissertação apresentada à Universidade de Aveiro para cumprimento dos requisitos necessários à obtenção do grau de Mestre em Engenharia Física, realizada sob a orientação científica do Professor Doutor Vítor José Babau Torres, Professor Catedrático do Departamento de Física da Universidade de Aveiro.

To my mother.

o júri / the jury

presidente / president

Prof.ª Dr.ª Teresa Maria Fernandes Rodrigues Cabral Monteiro
Professora Associada do Departamento de Física da Universidade de Aveiro

vogais / examiners committee

Prof. Dr. Vítor José Babau Torres
Professor Catedrático do Departamento de Física da Universidade de Aveiro

Prof. Dr. Ricardo Pedro Lopes Martins de Mendes Ribeiro
Professor Auxiliar do Departamento de Física da Universidade do Minho

acknowledgements

I would like to begin my acknowledgments by thanking my supervisor Prof. Vítor Torres for the opportunity and privilege for being one of his students. His guidance, patience, encouragement and his contributions are very much appreciated.
Second, I would like to thank my dear friend Sara Oliveira for helping me reviewing this text. Her knowledge in the English language is outstanding.
This dissertation is dedicated to my mother, for all her encouragement and support. She's the best mother a son could have.

palavras-chave modelação *ab initio*, defeitos, boro, silício, amorfo.

resumo

O presente trabalho tem como principal objectivo modelar os defeitos pontuais de boro em silício amorfo, usando um método *ab initio*, o código de teoria da densidade funcional – pseudopotencial (AIMPRO).

Os complexos de boro foram introduzidos em supercélulas de 64 átomos de silício. Os defeitos de boro foram estudados em 15 supercélulas diferentes. Estas supercélulas foram obtidas por um mecanismo de troca de ligação Wooten-Winer-Weaire por Ribeiro *et al.* (2010). Em média, as propriedades das 15 supercélulas estão de acordo com as distribuições radial e angular observadas, bem como as densidades electrónica e vibracional e com o espectro Raman.

Para confirmar este método, os defeitos mais simples de boro e o auto-intersticial no silício cristalino foram modelados. As principais conclusões estão em linha com os trabalhos de outros autores.

No silício amorfo foi muito difícil encontrar um verdadeiro auto-intersticial, visto que para a maioria das configurações testadas, a rede amorfa sofre uma ampla relaxação.

Verificou-se que o boro substitutional prefere a coordenação 4.

Foi confirmada a existência intrínseca de níveis localizados de “trapping” de buracos na rede amorfa não dopada, que pode explicar a baixa eficiência da dopagem com boro, como avançado por Santos *et al.* (2000). Os modos locais de vibração são, em geral, mais altos que os valores correspondentes na estrutura cristalina.

keywords *ab initio* modeling, defects, boron, amorphous, silicon.

abstract

The main goal of the current work is to model boron related point defects in amorphous silicon, using an *ab initio* method, the Density functional theory--pseudopotential code (AIMPRO).

The boron complexes were embedded in 64 silicon atom supercells. We have investigated the boron defects in 15 different supercells. These supercells were developed using a Wooten-Winer-Weaire bond switching mechanism by Ribeiro *et al.* (2010). In average, the properties of the 15 supercells agree with the observed radial and bond angle distributions, as well the electronic and vibrational density of states and Raman spectra.

To be confident with the method, the simplest boron defects and the self-interstitial in crystalline silicon were modeled. The main conclusions are in line with other authors' work.

In amorphous silicon it has been very hard to find a real self-interstitial, since for almost all the tested configurations, the amorphous lattice relaxes overall. We find that substitutional boron prefers to be 4-fold coordinated.

We find also an intrinsic hole-trap in the non-doped amorphous lattice, which may explain the low efficiency of boron doping, as advanced by Santos *et al.* (2010). The local vibrational modes are, in average, higher than the correspondent crystalline values.

Contents

List of Figures

List of Tables

Introduction

Crystalline silicon (c-Si) was first synthetized by French chemist Henri Deville in 1854 and since then has become one of the most studied materials by the scientific community. Since silicon is the second most available element on Earth's surface (after oxygen), it is relatively cheap, in comparison to other not so abundant semiconductors. However pure c-Si is very rarely found in nature. In nature, silicon forms compounds with other elements as with oxygen in silica.

The electric properties of semiconductors are highly influenced by the existence of defects and impurities. It is necessary to understand and control these properties in order to adapt semiconductors to industry's demands. This control is achieved mostly by doping the material with atoms from other elements.

Silicon atom is a group IV element of the periodic table and when c-Si is doped with atoms of an element from group V, it results in an excess of free electrons, which behave as charge carriers, making it a n-type material. Using the same analogy, when doped with atoms of a group III element, resulting in a deficiency of free electrons (equivalent to the formation of holes), c-Si became a p-type material. The border between the two types of materials is known as a p-n junction, the most crucial element in all the transistors and, inherently, in most electronic devices. Boron is by far the most widely used p-type dopant and therefore have been many studies of B related defects in c-Si (Adey 2003*a*, *b*, 2004; Wang, 2009)

The c-Si plays a major role in the electronics industry, but its high production cost lead us to search alternative materials with comparable characteristics. The amorphous silicon (a-Si), especially when passivated with hydrogen (a-Si:H), in the other hand, it lacks the well know advantages of c-Si, but it has some favorable properties of his own. a-Si can be prepared in large-area films onto a variety of substrates at a far lower cost than its crystalline counterpart.

In the crystalline form, all the atoms are fourfold coordinated, normally tetrahedrally bonded to four neighboring Si atoms. But in a-Si this long range order is not present and some of Si atoms are not fourfold coordinated (Laaziri *et al.*, 1999), existing dangling and floating bonds. The dangling bonds act as defects in the continuous random network and are traps for charge carriers, becoming the major drawback in a-Si application.

In the hydrogenated amorphous silicon (a-Si:H), hydrogen bonds to atoms with dangling bonds reducing the dangling bond density. This H passivation makes the material with sufficient low amount of defects to be used within devices, like in solar cells. However these solar cells still offer an efficiency way behind those produced with c-Si (Zallen, 1983).

There are many poorly understood phenomena associated with a-Si, like the low boron doping efficiency of B-doped a-Si (Stutzmann *et al.*, 1987) or the enhanced B diffusion in a-Si, which is far more severe than in c-Si (De Salvador *et al.*, 2008). Kong (2008, 2009) proposed that the enhanced B diffusion is due to a dangling-bond-mediated diffusion mechanism, but further studies in this and other phenomena are necessary.

In a previous work (Oliveira, 2008), the author studied the enhanced B diffusion in c-Si and in a SiGe alloy and then it was found out that the presence of germanium atoms did increase the migration barrier of B in agreement with experimental data (Bang *et al.*, 2007; Cowern *et al.*, 1994). This finding further motived us to extend this study to other materials such as a-Si and, perhaps in the near future, amorphous alloys like a-SiGe (Edelman *et al.*, 2008).

To achieve this proposed objective we started by studying the basic structural and electronic properties of B defects on the 15 different 64-atom a-Si samples, already obtained by Ribeiro *et al.* (2010). Since B diffusion in c-Si is enhanced by self-interstitials (Windl *et al.*, 1999) we also studied this defect, both in c-Si (to establish a baseline for the study) as well as in all a-Si samples.

The lack of structural order in a-Si requires, for a successful modeling, to test different conditions and consequently large number of computer jobs. So, for the self-interstitial modeling, an excess of 100 analysis runs were taken, spread across different sites and conditions in all 15 a-Si samples. This simple defect was not so simple to model, as we will further realize, since sometimes produced a new kind of amorphous structure and not the current sample with the intended defect within.

All major boron related point defects were also modeled, once again throughout all samples, including in c-Si. Hundreds of simulations were taken for all defects. We tried to replace the Si atom by a B atom in different conditions; in order to determine its preferable atomic coordination. We also focused our attention to the boron-silicon pair, in hopping to start to understand the B diffusion in a-Si (Kong *et al.*, 2008). In all previous simulations and when needed, spin polarization was performed.

In the following chapter we describe the main theoretical framework of the density functional theory. The modeling of the boron defects in the crystalline silicon is the subject of the chapter 2. The method for creating amorphous samples and the study of boron defects in amorphous silicon is discussed in chapter 3.

Chapter I
Theoretical Framework

1.1. The many-body problem

All the properties of a quantum mechanical system are within a wave function Ψ which obeys the Schrödinger equation

$$\hat{\mathcal{H}}\Psi = E\Psi \tag{1.1}$$

where E is the total energy of the system. The Hamiltonian operator ($\hat{\mathcal{H}}$) contains both kinetic ($\hat{T}$) and potential terms ($\hat{V}$)[1] from N_e electrons and N_n nuclei of the system,

$$\hat{\mathcal{H}} = \hat{T}_e + \hat{T}_n + \hat{V}_{ee} + \hat{V}_{en} + \hat{V}_{nn}, \tag{1.2}$$

where

$$\hat{T}_e = -\frac{1}{2}\sum_{i}^{N_e}\nabla_i^2, \tag{1.3}$$

$$\hat{T}_n = -\sum_{\alpha}^{N_n}\frac{1}{2M_\alpha}\nabla_\alpha^2, \tag{1.4}$$

$$\hat{V}_{ee} = \frac{1}{2}\sum_{\substack{i,j=1\\ i\neq j}}^{N_e}\frac{1}{\left|\mathbf{r}_i - \mathbf{r}_j\right|}, \tag{1.5}$$

$$\hat{V}_{en} = -\sum_{i,\alpha=1}^{N_e,N_n}\frac{Z_\alpha}{\left|\mathbf{r}_i - \mathbf{R}_\alpha\right|}, \tag{1.6}$$

$$\hat{V}_{nn} = \frac{1}{2}\sum_{\substack{\alpha,\beta=1\\ \alpha\neq\beta}}^{N_n}\frac{Z_\alpha Z_\beta}{\left|\mathbf{R}_\alpha - \mathbf{R}_\beta\right|}, \tag{1.7}$$

M_α, Z_α and $\mathbf{R}_\alpha$ represent the mass, charge and location of the α-th nucleus and $\mathbf{r}_i$ the coordinates of the i-th electron. Indexes n and e denote the nuclear and electronic terms, respectively. Thus, the wave function of the system is

$$\Psi(\mathbf{r},\mathbf{R}) \equiv \Psi\left(\mathbf{r}_1, s_1, ..., \mathbf{r}_{N_e}, s_{N_e}; \mathbf{R}_1, ..., \mathbf{R}_{N_n}\right), \tag{1.8}$$

[1] Note that all quantities herein are expressed in term of atomic units unless stated otherwise.

where s is the electron spin. Therefore Ψ is function of $3N_n + 4\sum_\alpha Z_\alpha$ scalar variables, which implies that solving even the simplest problem is impractical, even with the fastest and more powerful computers currently available. It became necessary to find a method by means of approximations, always bearing in mind the need to maintain the reliability of results.

1.2. The Born-Oppenheimer approximation

Since the mass of an electron is several orders of magnitude less than the mass of the nucleus it is reasonable to assume that the electrons react instantaneously to the movement of the nuclei. Born and Oppenheimer (1927) thus proposed that the total wave function $\Psi(\mathbf{r},\mathbf{R})$ is given by

$$\Psi(\mathbf{r},\mathbf{R}) = \psi_{\mathbf{R}}(\mathbf{r})\Phi(\mathbf{R}) \tag{1.9}$$

where ψ_{R} and Φ represent the wave functions of electrons and nuclei, respectively, and the index R indicates that the electronic wave function is determined for a given fixed configuration of nuclei.

Combining the last equation with the Schrödinger equation (1.1), we get the equation involving electrons,

$$\left(\hat{T}_e + \hat{V}_{ee} + \hat{V}_{en}\right)\psi_{\mathrm{R}}(\mathbf{r}) = E_e\psi_{\mathrm{R}}(\mathbf{r}) \tag{1.10}$$

and the equation involving the nuclei,

$$\left(\hat{T}_n + \hat{V}_{nn} + E_e(\mathbf{R}) + C(\mathbf{R})\right)\Phi(\mathbf{R}) = E\Phi(\mathbf{R}), \tag{1.11}$$

where

$$C(\mathbf{R}) = -\sum_{\alpha}^{N_n}\frac{1}{2M_\alpha}\left[\Phi(\mathbf{R})\nabla_\alpha^2\psi_{\mathbf{R}}(\mathbf{r}) + 2\nabla_\alpha\psi_{\mathbf{R}}(\mathbf{r})\cdot\nabla_\alpha\Phi(\mathbf{R})\right]. \tag{1.12}$$

This term $C(\mathbf{R})$, for the majority of cases, is almost negligible due to the heavy mass of the nuclei. The Born-Oppenheimer approximation considers $C(\mathbf{R}) = 0$. The electronic state of the n-body problem is usually defined after a determined function ψ_{R} for a fixed set of atomic positions.

1.3. Variational principle

There are two distinct methods of obtaining a stationary solution of the Hamiltonian – a grid method and a variational method. The first integrates a Schrödinger wave function using discrete methods, while the second uses a variational principle as described here. In this method, there is *hand-picked* subspace $\{\phi_1,...,\phi_M\}$ from the Hillbert space to get a rough function Ψ_{app} of the wave function Ψ_0,

$$\Psi_0 \approx \Psi_{\text{app}} = \sum_i^M c_i \phi_i \,. \tag{1.13}$$

The variational principle states that the expected value for the total energy E, functional of the wave function Ψ_{app}, has a minimum value,

$$E\left[\Psi_{\text{app}}\right] = \frac{\int \Psi_{\text{app}}^* \hat{\mathcal{H}} \Psi_{\text{app}} dr}{\int \Psi_{\text{app}}^* \Psi_{\text{app}} dr} \,. \tag{1.14}$$

Hence the approximated value of the total energy is

$$E_{\text{app}} = E\left[\Psi_{\text{app}}\right] = \left[\sum_{i,j=1}^M c_i^* c_j H_{ij}\right] \Big/ \left[\sum_{i,j=1}^M c_i^* c_j S_{ij}\right], \tag{1.15}$$

where $H_{ij} = \int \phi_i^* \hat{\mathcal{H}} \phi_j dr$ and $S_{ij} = \int \phi_i^* \phi_j dr$. For the ground-state the derivative of E_{app} with c_i should vanish implying that,

$$\sum_{j=1}^M \left(H_{ij} - E_{\text{app}} S_{ij}\right) c_j = 0 \text{, for } i = 1,...,M \,. \tag{1.16}$$

1.4. Hartree-Fock Theory

Taking into account the Pauli principle, the electronic functions in (1.13) must be antisymmetric. Conveniently, using single-particle wave functions, the antisymmetry may be obtained in the form of a Slater determinant (Slater, 1929),

$$\psi_{\mathbf{R}}^{HF}(\mathbf{r}) = \frac{1}{\sqrt{N!}} \det \begin{bmatrix} \psi_1(r_1) & \cdots & \psi_N(r_1) \\ \vdots & \ddots & \vdots \\ \psi_1(r_N) & \cdots & \psi_N(r_N) \end{bmatrix}. \tag{1.17}$$

The determinant ensures the antisymmetry since exchanging two of the single electron spin-orbitals will change $\psi_{\mathrm{R}}(\mathbf{r})$ by a factor of -1 while the presence of two identical spin-orbitals will result in $\psi_{\mathrm{R}}(\mathbf{r})=0$.

Considering $\psi_{\mathbf{R}}^{HF}(\mathbf{r})$ a solution to the Hamiltonian from the system in (1.10) and (1.11), minimizing the total energy, subject to the orthogonality condition $\int \psi_i^* \psi_j dr = \delta_{ij}$, gives the Hartree-Fock equations (Mc Weeney, 1989; Thijssen, 1999),

$$\hat{F}\psi_i(r) = \sum_{j=1}^{N} \varepsilon_{ij}\psi_j(r). \tag{1.18}$$

The Fock operator $\hat{F}$ is given by,

$$\hat{F} = \hat{h} + \hat{j} - \hat{k} \tag{1.19}$$

in with $\int \psi_i^* \hat{h} \psi_i dr = H_i$ includes the kinetic energy from the electrons and the potential energy from the electron-nucleus interaction. The potential energy from the interaction between electrons is translated by the terms $\hat{j}$ and $\hat{k}$,

$$\hat{j} = \sum_{k=1}^{N} \int \frac{\psi_k^*(\mathbf{r}_2)\psi_k(\mathbf{r}_2)}{|\mathbf{r}_1 - \mathbf{r}_2|} dr_2 \tag{1.20}$$

and

$$\hat{k} = \sum_{k=1}^{N} \int \frac{\psi_k^*(\mathbf{r}_2)\psi_k(\mathbf{r}_1)}{|\mathbf{r}_1 - \mathbf{r}_2|} dr_2 . \tag{1.21}$$

The term $\hat{j}$ expresses the mean Hartree field and $\hat{k}$ expresses the exchange field, which arises due to the antisymmetry of the wave functions.

The matrix ε in equation (1.18) is composed of Lagrange multipliers from the minimization process. The diagonal elements are given by,

$$\varepsilon_i = \varepsilon_{ii} = \left\langle \psi_i \middle| \hat{F} \middle| \psi_i \right\rangle = H_i + \sum_{j=1}^{N} \left(J_{ij} - K_{ij} \right) \tag{1.22}$$

which results in the following expression for the energy of the system,

$$E = \sum_{i}^{N} \varepsilon_i - \frac{1}{2} \sum_{i,j=1}^{N} \left(J_{ij} - K_{ij} \right) \tag{1.23}$$

It is typical in a computational implementation of the Hartree-Fock theory that the spin-orbitals ψ_i are expressed as a linear combination of the atomic orbitals. After careful choice of a set of M functions $\phi_i(\mathbf{r})$,

$$\psi_j(\mathbf{r}) = \sum_i^M c_{ij}\phi_i(\mathbf{r}) \tag{1.24}$$

The matrix form of the Fock equation leads to the generalized eigenvalue equation, known as the Roothaan equation (Roothaan, 1951),

$$\mathbf{F}\cdot\mathbf{c}_j = \varepsilon_j \mathbf{S}\cdot\mathbf{c}_j \tag{1.25}$$

where $\mathbf{S}$ is a $M \times M$ matrix, $S_{ij} = \langle \phi_i | \phi_j \rangle$. The last equation is solved self-consistently until the both the wave function and the corresponding total energy converge. Koopmans (1934) gave physical meaning to the eigenvalues ε_i.

1.5. Density Functional Theory

The Density Functional Theory (DFT) (Hohenberg and Kohn, 1964; Kohn and Sham, 1965), considers the total energy as a functional of electron charge density $n(\mathbf{r})$ rather than a composition of single electron wave functions as in the Hartree-Fock theory.

$$n(\mathbf{r}) = \sum_{i=1}^N |\psi_i(\mathbf{r})|^2 \tag{1.26}$$

1st Hohenberg-Kohn theorem *The external potential is a unique functional of the electron charge density* $n(\mathbf{r})$ *(Hohenberg and Kohn, 1964).*

The total energy of the system is given by,

$$E[n] = F[n] + \int \upsilon_{ext}(\mathbf{r}) n(\mathbf{r}) d\mathbf{r} \tag{1.27}$$

where υ_{ext} is the external potential experienced by electrons due to, for example, the nucleus-electron interactions, and F is a system-independent functional that takes into account the electron kinetic energy, the Hartree energy, the electron correlation energy and the exchange-correlation energies.

2nd Hohenberg-Kohn theorem *For an electron charge density* $\tilde{n}(\mathbf{r})$ *such that* $\tilde{n}(\mathbf{r}) \geq 0$ *and* $\int \tilde{n}(\mathbf{r})\, d\mathbf{r} = N$*, the ground state energy* E_0 *is the lowest energy value (Hohenberg and Kohn, 1964),*

$$E_0 \leq E[\tilde{n}]. \tag{1.28}$$

A significant simplification comes from the use of the electron charge density, since this method, unlike the Hartree-Fock theory, has no approximations. However the contribution of exchange-correlation to the functional F keeps being non-local and usually unknown.

1.5.1. Kohn-Sham equations

Implementing DFT transforms the Schrödinger equation for many electrons [equation (1.10)] in a system of single-particle equations, which are the Kohn-Sham equations (Kohn and Sham, 1965),

$$\left[-\frac{1}{2}\nabla^2 - \sum_{\alpha} \frac{Z_\alpha}{|\mathbf{r} - \mathbf{R}_\alpha|} + \int \frac{n(\mathbf{r}')}{|\mathbf{r} - \mathbf{r}'|} d^3\mathbf{r}' + \frac{\delta E_{XC}[n]}{\delta n(\mathbf{r})} \right] \psi_\lambda(\mathbf{r}) = \varepsilon_\lambda \psi_\lambda(\mathbf{r}), \tag{1.29}$$

where the charge density n is obtained from (1.26).

The first three terms of the equation (1.29) express the kinetic energy, the external potential imposed by the ions (nuclei) and the Hartree energy, respectively. The fourth term adds the effects of the remaining bodies in the system in the form of an exchange-correlation functional. The strength of DFT comes from the fact that there is a universal density functional E_{XC} (which depends solely on the electron charge density n) allowing the exact solution of the charge density and total energy of a system in its ground-state to be obtained.

The total energy functional for a system with many electrons is given by (Parr and Yang, 1989),

$$E[n] = \sum_{\lambda=1}^{N} \varepsilon_\lambda - J[n] + E_{XC}[n] - \int V_{XC}[n] n(\mathbf{r})\, d\mathbf{r} \tag{1.30}$$

In equation (1.30), the Hartree energy and the exchange-correlation potential (J and V_{XC}, respectively) are given by

$$J[n] = \frac{1}{2} \int \frac{n(\mathbf{r}) n(\mathbf{r}')}{|\mathbf{r} - \mathbf{r}'|} d\mathbf{r} d\mathbf{r}' \tag{1.31}$$

$$V_{XC}[n] = \frac{\delta E_{XC}[n]}{\delta n(\mathbf{r})}. \tag{1.32}$$

The Kohn-Sham equations (1.29) are solved self-consistently, until convergence is achieved. First, an initial charge density is chosen and equation (1.29) is solved. The resulting eigenvectors serve as a starting point for the equation (1.26), generating a new charge density, repeating the cycle again, until it is found that the charge density does not change significantly, so the method is self-consistent.

Until know the DFT is still exact but the exact form of E_{XC} is unknown. Some approximations are currently used to overcome this. In fact, the demand for the exact form of this functional still remains an actual research topic (Doren *et al.*, 2001, Tao *et al.*, 2008).

The previous formalism neglects the dependence of the electron spin, apart from the term E_{XC}. Considering the electron charge density as the superposition of spin-up and spin-down charge densities $n(\mathbf{r}) = n_{\uparrow}(\mathbf{r}) + n_{\downarrow}(\mathbf{r})$, the spin is then accounted for (von Barth and Hedin, 1972; Rajogopal and Callaway, 1973).

1.5.2. The exchange correlation functional

A common approach to circumvent the problem of not knowing E_{XC} is called the Local Density Approximation (LDA) and the one that considers the electron spin is the Local Spin Density Approximation (LSDA) (Kohn and Sham, 1965; von Barth and Hedin, 1972; Perdew and Zunger, 1981). The exchange-correlation energy is assumed to be local and usually distinguished in two contributions, the exchange energy E_X and correlation energy E_C :

$$E_{XC}[n_{\uparrow}, n_{\downarrow}] = E_X[n_{\uparrow}, n_{\downarrow}] + E_C[n_{\uparrow}, n_{\downarrow}], \tag{1.33}$$

using LSDA notation. The analytical form of the exchange functional of a homogeneous electron gas is (von Barth and Hedin, 1972),

$$E_X[n_{\uparrow}, n_{\downarrow}] = -\frac{3}{2}\left(\frac{3}{4\pi}\right)^{1/3}\left(n_{\uparrow}^{4/3} + n_{\downarrow}^{4/3}\right) \tag{1.34}$$

The correlation term is more complex because it involves the use of the perturbation theory for a high-density regime (Perdew and Zunger, 1981), while for low density the Monte Carlo method is used, applied to a Green function (Ceperly, 1978; Ceperly and Alder, 1980). Several

functional in the parameterized form have been presented by Perdew and Zunger (1981) (PZ), Vosko *et al.* (1980) (VWN) and Perdew and Wang (1992) (PW).

A more accurate estimate of the exchange-correlation energy is obtained by taking the first order expansion of E_{XC} in charge density and thus includes the terms dependent on the gradient of charge density ∇n (Perdew, 1991; Perdew *et al.* 1996*a*, *b*). This method is known as the Generalized Gradient Approximation (GGA).

1.6. Pseudopotencials

The chemical properties of an atom are almost exclusively due to the valence electrons and their interaction with the atoms, while the core states are relatively independent of the environment where the atom is. The core electrons may be eliminated in the system equation, considering that valence electrons in each atom interacting with the nucleus and the core electrons via an effective potential, called pseudopotential.

The use of pseudopotentials has the advantage, compared to calculations using all electrons, of reducing the number of electrons to treat, since the core electrons are not considered.

Detailed information on the pseudopotencial method has been extensively reported (Harrison, 1966; Brust, 1968; Stoneham, 1975; Heine, 1970; Pickett, 1989).

The calculations presented in the proceeding chapters employ the Hartwigsen-Goedecher-Hutter (HGH) pseudopotentials (Hartwigsen *et al.*, 1998).

1.7. Boundary conditions

Putting a defect in a supercell has a major consequence. The objective is to model the defect, but in the supercell run, the defect is replicated for each cell, consequence of the periodic boundary conditions. Note that this happens whether the defect is modeled in c-Si or in a-Si and, particularly in c-Si, does not matter where we put the defect – in the case of a substitucional impurity with an offset of $\delta\mathbf{r}$ implicates that all the replicas of that impurity will be moved fowling the same vector. If the supercell does not have an adequate size or volume, some non-realistic defects may occur, mainly caused by elastic, coulombic, dipolar or quadrapolar interaction between replicas of the defects. Calculations presented in the proceeding chapters all employ the supercell method. Supercells of 64 atoms where tested and found to give converged results.

The AIMPRO code can also implement the cluster method where the cell is not replicated. In this run, the interactions between defects do not occur but an unintended interaction between defect and the surface is common.

1.8. Basis functions

The AIMPRO LDA DFT code used throughout this dissertation employs a real-space Gaussian type basis set (Jones and Briddon, 1999). One problem with the supercell approach however is that the requirement of integration over the Brillouin-zone (BZ) makes an expansion of the wave function in a reciprocal space necessary.

Block basic functions $B_{\mathbf{k}i}(\mathbf{r})$ are constructed from Gaussian functions[2] ϕ_i centered at the atomic sites $\mathbf{R}_i$ with N_L lattice vectors $\mathbf{L}_\mathbf{n}$,

$$B_{\mathbf{k}i}(\mathbf{r}) = \frac{1}{\sqrt{N_L}} \sum_{\mathbf{L}_\mathbf{n}} \phi_i(\mathbf{r} - \mathbf{R}_i - \mathbf{L}_\mathbf{n}) e^{i\mathbf{k}\cdot\mathbf{L}_\mathbf{n}}, \tag{1.35}$$

where $\mathbf{k}$ is a reciprocal space vector within the BZ. The localized orbitals are given by,

$$\phi_i(\mathbf{r}) = (x - R_{ix})^{l_1} (y - R_{iy})^{l_2} (z - R_{iz})^{l_3} e^{-a_i(\mathbf{r}-\mathbf{R}_i)^2}, \tag{1.36}$$

with *s*-, *p*- or *d*-like orbitals corresponding to $\sum_i l_i = 0,1$ or 2. The Kohn-Sham orbitals $\psi_{\mathbf{k}\lambda}$ are then expanded over all $B_{\mathbf{k}i}(\mathbf{r})$ basis functions,

$$\psi_{\mathbf{k}\lambda}(\mathbf{r}) = \sum_i c_{\mathbf{k}\lambda,i} B_{\mathbf{k}i}(\mathbf{r}) \tag{1.37}$$

with the $\mathbf{k}\lambda$ pair labeling the state. The charge density is readily obtained as

$$n(\mathbf{r}) = \sum_{i,j,\mathbf{k}} b_{ij}(\mathbf{k}) B^*_{\mathbf{k}i}(\mathbf{r}) B_{\mathbf{k}j}(\mathbf{r}) \tag{1.38}$$

$$b_{ij}(\mathbf{k}) = \sum_\lambda f_{\mathbf{k}\lambda} c^*_{\mathbf{k}\lambda,i} c_{\mathbf{k}\lambda,j} \tag{1.39}$$

where $f_{\mathbf{k}\lambda}$ is the occupancy of the $\mathbf{k}\lambda$ state, and this should be 2 for a filled level and 0 for an empty one.

[2] Expressed in Cartesian coordinates.

The advantage of Guassian-like functions is that their integrals can be found analytically, in contrast to another popular choice of basis functions (Jones and Briddon, 1999). However, they are not orthogonal, and over-completeness can induce numerical instabilities.

1.9. *Brillouin-zone sampling*

In the supercell method, integration over the Brillouin-zone is required in the calculation of physical quantities like total energy, charge density or density of states, amongst others. The integrand function $f(\mathbf{k})$ is periodic in reciprocal space, and has no simple analytic form. Several schemes were proposed to avoid numerical integration over a dense mesh. In the scheme from Baldereschi (1973) and Chadi and Cohen (1973), one or a set of N *special* k_i-points can be used to obtain the average $\overline{f}$ over the BZ of volume $(2\pi)^3/\Omega$, where

$$\overline{f} = \frac{\Omega}{(2\pi)^3}\int f(\mathbf{k})\,d\mathbf{k} \approx \frac{1}{N}\sum_i^N f(\mathbf{k}_i). \tag{1.40}$$

A clearer scheme was proposed by Monkhorst and Pack (1976); Pack and Monkhorst (1977) (MP) because the last method, despite the obvious advantages over a full integration, did not provide an obvious way of checking the convergence of the calculations.

In the MP scheme the *special* k-points are a grid of $I\times J\times K$ points in reciprocal space given by,

$$\mathbf{k}(i,j,k) = u_i\mathbf{g}_1 + u_j\mathbf{g}_2 + u_k\mathbf{g}_3 \tag{1.41}$$

where $\mathbf{g}_1$, $\mathbf{g}_2$ and $\mathbf{g}_3$ are the reciprocal space unit-vectors and u_i, u_j and u_k are given by,

$$u_i = (2i - I - 1)/2I, \qquad (i = 1,\ldots,I) \tag{1.42}$$
$$u_j = (2j - J - 1)/2J, \qquad (j = 1,\ldots,J) \tag{1.43}$$
$$u_k = (2k - K - 1)/2K, \qquad (k = 1,\ldots,K) \tag{1.44}$$

with I, J and $K \geq 1$. When $I = J = K$ the sampling scheme is referred to as $MP - I^3$. Convergence is ensured by increasing the values of I, J and K until the calculated value or property of interest does not change significantly.

In a high symmetry supercell some of the k-points may be equivalent due to the symmetry operations associated with that supercell. In this case the redundant k-points may be removed and the equivalent one that is left will be weighted accordingly.

In the proceeding chapters a 2^3 MP sampling scheme was used, except otherwise noted. This MP sampling showed sufficient convergence.

1.10. Ewald summations

Series like $1/r^p$ with $p \leq 2$ converge very slowly as r goes to infinity and so to calculate Coulombic and dipolar interactions it is necessary to evaluate slowly converging sums. To solve this problem, Ewald (1921) proposed a method in which the series is split into a fast-converging and slow-converging parts,

$$\sum_L \frac{1}{r_L^p} = \sum_L \frac{\operatorname{erfc}(\alpha r_L)}{r_L^p} + \sum_L \frac{\operatorname{erf}(\alpha r_L)}{r_L^p}. \tag{1.45}$$

Evaluation of the first term is straightforward as $\operatorname{erfc}(x)$ converges to zero when $x \to \infty$. The last term, slowly converging in real-space, is Fourier transformed, and as a consequence its terms are now sort-ranged and fast converging in reciprocal space. The parameter α controls the transition between the real-space and reciprocal-space sums. Although the analytical result does not depend on the choice of α in practice this is not the case. This is a consequence of the sums only covering a finite set of lattice vectors. An extensive treatment of this method was given by Leeuw *et al.* (1980). This method is used in AIMPRO to separate and include the local and non-local contributions of the pseudopotencial.

1.11. Calculation of observables

The DFT is an exact ground-state theory. Thus, the properties of excited states (including unoccupied electron energy levels) are outside the scope of DFT calculations. In fact it is the subject of the time-dependent DFT (Runge and Gross, 1984; Marques and Gross, 2004). However there are many fundamental properties that DFT can successfully model and whose objectives are to predict or confirm the experimental data. This section explains how the most important of these properties are obtained.

1.11.1. Local structure / Forces

Once the Kohn-Sham equations are solved for a charge density of a consistent configuration of atoms is desirable to know what forces act on each atom. The force F_α exerted on an atom is simply equal to $-\nabla_\alpha E$ (Hellman-Feynman's theorem) (Hellmann, 1937; Feymann, 1939) and thus

slightly displacing every atom of his position, and calculating ΔE, the force exerted on each atom can be calculated.

Varying the position of the ions causes a variation of the charge density which can cause two results: a change in $b_{ij}(\mathbf{k})$ and a change in the basis functions $B_{\mathbf{k}i}$. Once all contributions to ΔE are considered, from the force acting on each atom, it is known that the atoms can move according to these forces. In an iterative way, this movement is made until the variation of forces and the change in total energy are negligible. It is said then that the structure is *relaxed*. The AIMPRO makes use of a conjugate gradient algorithm, which means that the atoms are moved in the direction where there was a component of the forces obtained in the previous iteration, as well as along the component of the forces obtained in the current iteration. The distance that the atom moves in this direction is chosen approximating a cubic or quadratic function that expresses the energy variation with position. But it is important to stress that this simplistic approach implies that the *relaxed* structure will be located in a local minimum of the total energy surface. There is no guarantee that is located in the global minimum. To ensure, as far as possible, that the structure is *relaxed* in a global minimum is necessary to initiate the structural optimization from several different initial configurations.

1.11.2. Total Energy

One of the most fundamental properties of a system is it total energy E_T, equation (1.30). It is frequently used to compare the energy of similar systems. In this case a similar system is that containing the same number of atoms of each species (defined by the corresponded pseudopotential) and the same overall charge. If these conditions are not met then it is necessary to compare formation energies instead.

1.11.3. Derived Properties

Formation Energy

The chemical potential μ_s of a species s is defined as the derivative of the Gibbs free energy (Reif, 1965; Flynn, 1972),

$$G = E + PV - TS\,. \tag{1.46}$$

Under thermodynamic equilibrium, μ_s is equal over the entire system, regardless of any differences in phase and hence is equivalent to the free energy per particle. Neglecting the term

PV which is small for solid state reactions and the term $-TS$ that is quite small at low temperatures, the formation energy is given by,

$$E_f = E_T + q\mu_e - \sum_s n_s \mu_s \tag{1.47}$$

where E_T is the total energy of the system, q is the system's charge state, n_s is the number of atoms of species s and μ_s is the chemical potential corresponding to that species. The electron chemical potential μ_e is usually taken to be,

$$\mu_e = E_F + E_\upsilon \tag{1.48}$$

where E_F is the Fermi energy relative to E_υ which is the energy of the highest occupied orbital, usually taken from the Kohn-Sham levels. Alternatively E_υ can be obtained by comparing $E_T(q=-1)$ to $E_T(q=0)$.

The formation energy is a quantity that provides access to a great deal of information. By taking into account the chemical potentials, it is possible to compare supercells of different sizes and to compare the stability of defects containing different numbers of each species (useful to calculate binding energies). Comparing the formation energy of a given defect, for different charged states, gives the electrical levels. The formation energy can also be used to calculate the solubility of a defect.

Binding Energies

When a defect can be considered to be formed by two or more primary defects it is often useful to know what the cohesive energy is between the constituents. The binding energy E_B of the complex C formed by two constituents A and B is given by

$$E_B = E_f^A + E_f^B - E_f^C \tag{1.49}$$

where E_f^A and E_f^B are the formation energies of the constituents that make up the complex C and E_f^C the corresponding formation energy of the complex.

An alternative way to calculate the binding energy is to build a series of supercells in which the constituents A and B are initially close together (in the form of the complex C) and in the following cells they are gradually separated. By comparing the energies of these supercells, we obtain the energy as a function of separation A and B. If the energy reaches an asymptotic limit for greater separation then the binding energy is the difference between the energy of the

supercell containing separate A and B, and the energy of supercell containing the complex C. This method is more accurate than the method using the formation energy, especially when the supercells are equally charged, as is usually the case, since to first order the strain and the quadrupolar interactions between neighboring cells will be equal for each separation and hence cancel each other out.

Migration Energy

The basic principle to determine the migration energy of an atom or complex is extremely simple. The AIMPRO is capable of implementing several methods for this calculation, yet the NEB (Nudged Elastic Band) method is by far the most commonly used.

The NEB determines the lowest energy path between an initial and a final configuration of atoms. This path is very important in the study of the diffusion of defects and is often called minimum energy path (MEP).

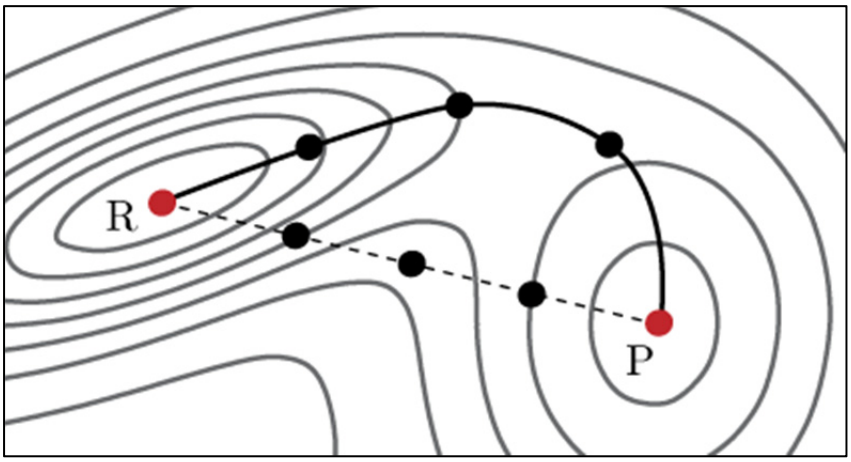

Fig. 1 Contour plot for the energy surface with R and P configurations represented.

Considering the *relaxed* configurations R and P, we intended to determine the MEP in this case. To start the algorithm that implements the NEB in AIMPRO, it is necessary to define settings and intermediate between, for example, by simple linear combination (dashed path in figure 1).

This method considers that all configurations between R and P, including these, are linked by a force with elastic constant $k \neq 0$. Iteratively, NEB runs thru all the initial images (initial path) and evaluates a new position for the intermediate configurations (images) taking into account two criteria: a) the force acting perpendicular to the path between the images and b) the cohesive elastic force that keeps the settings in the path. Gradually these operations will bring the desired method to the MEP (non-dashed path in figure 1).

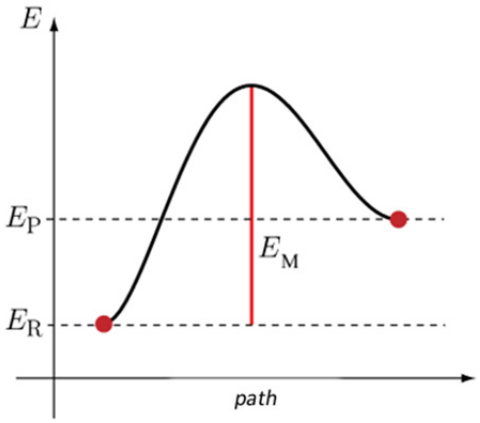

Fig. 2 Minimum Energy Path (MEP).

The representation of the MEP determined by NEB (figure 2) shows a diffusion barrier. The height of the energy barrier E_M is the migration energy of the defect. However this method has the same problem regarding the local minimum, as discussed earlier. To ensure that the appropriate MEP was reached, we must repeat the process for different initial paths (i.e., for different initial images).

Thermal stability

Many experimental techniques are able to observe at what temperature a defect disappears, so it is desirable to estimate the thermal stability of a defect. Assuming that a complex, when subjected to heat treatment (annealing), dissociates and does not undergo any reaction with other mobile species at the annealing temperature, it becomes straightforward to estimate the thermal stability. The rate at which the complex dissociates is

$$R = \nu \exp\left(\frac{-E_A}{kT}\right) \tag{1.50}$$

where ν is a given frequency, k is the Boltzmann constant and T is temperature. E_A is the activation energy of the defect, which is approximately the sum of the formation energy of the defect and the migration energy of the species that diffuses, and can be calculated using the AIMPRO. The frequency in (1.50) is usually the Debye frequency, another property that can be determined by means of *ab initio* modeling, however this operation is a complex one.

Electrical levels

The formation energy of charged defect is a function of the electronic chemical potential or equally to the Fermi level. The formation energy of a complex or defect can then be calculated as a function of E_F for different charged states. For a given value of E_F, one of the states will have the minimum energy value, thus being the most stable. The value of E_F for which two charged states are equal in energy corresponds to an occupancy level. In other words, the energy value E_F for which $E_f(q) = E_f(q+1)$ corresponds to the level $(q/q+1)$ of the defect. When E_F is greater than its critical value, the defects will be at the charged state q and when E_F is at its lowest value, the defect will be at the charged state $(q+1)$. This method for calculating the energy levels is known as the Formation Energy Method.

However it is customary to use the Marker Method (Coutinho *et al.*, 2002). This method was used in this dissertation and it can calculate the electrical levels with a better precision by solving the following equation,

$$E_d(q) - E_d(q+1) + E_d(q/q+1) = E_m(q) - E_m(q+1) + E_m(q/q+1) \qquad (1.51)$$

where $E_d(q)$ and $E_d(q+1)$ are the energies of defect in states q and $(q+1)$. $E_d(q/q+1)$ is the position of the $(q/q+1)$ level of the defect. $E_m(q)$ and $E_m(q+1)$ are the energies of the marker defect in the respective states. Ideally the defect marker must have similar electrical properties to the defect under study and should have a level $(q/q+1)$ whose energy $E_m(q/q+1)$ is known. Knowing the value $E_m(q/q+1)$ and calculating $E_m(q)$, $E_m(q+1)$, $E_d(q)$ and $E_d(q+1)$ the equation (1.51) is solved and the value of $E_d(q/q+1)$ determined. Often the Marker Method has a numerical error not greater than $0.2\ eV$. This method is however more reliable due to the cancellation of the errors that arise from interactions between supercells. The calculation of electric levels is critical to identify electrically active defects.

Vibrational Modes

The vibrational modes of a crystal or defect are given by the system's dynamical matrix $\mathbf{D}$ (Born and Huang, 1954) by solving the eigenvalue problem

$$\mathbf{D} \cdot \mathbf{U} = \omega^2 \mathbf{U}\,, \qquad (1.52)$$

where the $3N$ eigenvalues ω^2 are the square frequencies associated with the $3N$ normal modes $\mathbf{U}$. Each normal mode is a $3N$ dimensional vector describing the motion for all N atoms for that mode. The $3N \times 3N$ elements of the matrix $\mathbf{D}$ are given by,

$$D_{ab}(i,j) = \frac{1}{\sqrt{M_i M_j}} \left. \frac{\partial^2 E}{\partial u_{ia} \partial u_{jb}} \right|_0 \tag{1.53}$$

where a and b are any of the three Cartesian coordinates and u_{ia} and u_{jb} are the displacements of atoms having mass M_i and M_j respectively, in those directions.

The calculation of the second derivatives in equation (1.53) is achieved by the following numerical method. First, the supercell must be *relaxed*, turning all the forces effectively to zero. Then the atom i is moved a small amount ε (~ 0.025 a.u.) along the Cartesian direction a. The new charge density is then calculated and from that the forces, now different from zero since the structure has been perturbed. We label $f_{bj}^{+}(a,i)$ as the new component of the force that act on the atom j, in the Cartesian direction b. The atom i is then moved the same distance in the opposite direction $-\varepsilon a$, resulting in a force $f_{bj}^{-}(a,i)$. The second derivative of the energy is then,

$$\left. \frac{\partial^2 E}{\partial u_{ia} \partial u_{jb}} \right|_0 = \frac{\partial}{\partial u_{ia}} \frac{\partial E}{\partial u_{jb}} = \frac{\partial}{\partial u_{ia}} \left(-f_{bj} \right) = \frac{f_{bj}^{-}(a,i) - f_{bj}^{+}(a,i)}{2\varepsilon} \tag{1.54}$$

This way of computing the second derivative of energy includes some non-harmonic contributions. For this reason, the frequencies obtained in this manner are often referred to as *quasi*-harmonic frequencies (Jones *et al.*, 1994).

When the impurities, such as boron in silicon, are lighter than the atoms of the network, the vibration modes are greater than the crystal. In this case we get a local vibrational mode (LVM) where only the impurity and its nearest neighbors vibrate. Therefore, we get great results by taking into account only the second derivatives for the impurity and its nearest neighbors.

The vibrational modes of a defect can be calculated and compared with results of infrared spectroscopy and photoluminescence. As the frequencies of vibration modes are extremely sensitive to the structure of a defect, if we compare the experimental data with the modeled one, and they are consistent then there is a strong possibility that the observed and modeled structure are the same. Advances in the study of isotopic impurities and pressure effects have led to better identification of defects.

Chapter II
Boron Defects in Crystalline Silicon

Boron is the most important p-dopant in silicon, therefore boron complexes in crystalline silicon has been investigated, using DFT computational codes (Adey, 2004). One of the most successful and employed in boron c-Si studies is the AIMPRO code, which has been developed for the last 20 years by R. Jones and P. R. Briddon.

Whatever, very few studies have been conducted in a-Si using DFT codes. To guide the studies of boron a-Si is essential to understand the basic principles of *ab initio* studies in c-Si so we hope to carry out successful studies in amorphous materials. In this chapter the simplest, but convenient, boron complexes in c-Si are reexamined, and the study of B related defects in a-Si is the subject of the next chapter.

2.1 Supercell characterization

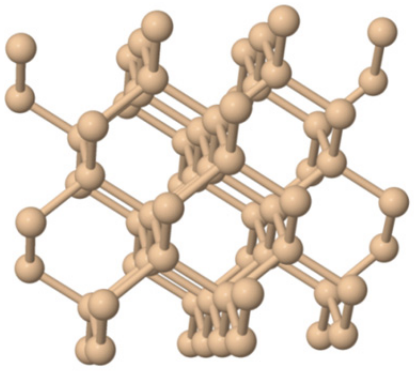

Fig. 3 64-atom cubic silicon supercell.

The boron defect embedded in a 64-atom supercell (figure 3) was used in the proceeding simulations. The silicon and boron species was characterized by the respective HGH pseudopontential (Hartwigsen *et al.*, 1998). As stated in the last chapter a $2 \times 2 \times 2$ MP sampling was used. All the studies were performed using LDA, but when needed, a spin polarization was applied.

State equation

The AIMPRO enable us to calculate all variables in the Birch-Murnaghan equation of state (Murnaghan, 1944; Birch, 1947),

$$E[V] = E_0 + \left[\frac{(V_0/V)^{B_0'}}{B_0' - 1} + 1 \right] \frac{B_0 V}{B_0'} - \frac{B_0 V_0}{B_0' - 1}. \quad (2.1)$$

In the previous equation, V is the volume of the supercell, $B_0 = -V\left(\partial P/\partial V\right)_T$ is known as the bulk modulus and B_0' its first derivative over pressure. The table below show that all obtained parameters are in agreement with previous calculated and experimental data.

Table 1 Calculated parameters for c-Si compared with previous calculated (Oliveira, 2008) and experimental data. The determined lattice constant a_0 is compared with the experimental value from James and Lord (1992). The experimental value for bond length r_0 was taken from Brenner *et al.* (1991). The bulk modulus and its derivative are compared with experimental data from Singh (1993) and Beattie and Schirber (1970), respectively.

Parameters	calculated	Oliveira (2008)	experimental
a_0 (Å)	5.39	5.40	5.43
r_0 (Å)	2.34	2.34	2.35
B_0 (GPa)	96.65	94.60	97.9
B_0'	4.12	3.94	4.09

Band structure

As shown in the figure 4, AIMPRO package is able to determine the band structure. Our calculation for c-Si is in agreement with other calculations like the one determined using the non-local pseudopotential method by Chelikowsky and Cohen (1976). The indirect band gap in c-Si is reproduced, but the energy gap is underestimated (proximally 50% underestimation), which is a well-known DFT drawback. In this case a $0.52\ eV$ band gap was determined against the $\sim 1.15\ eV$ experimental value (Low *et al.*, 2008).

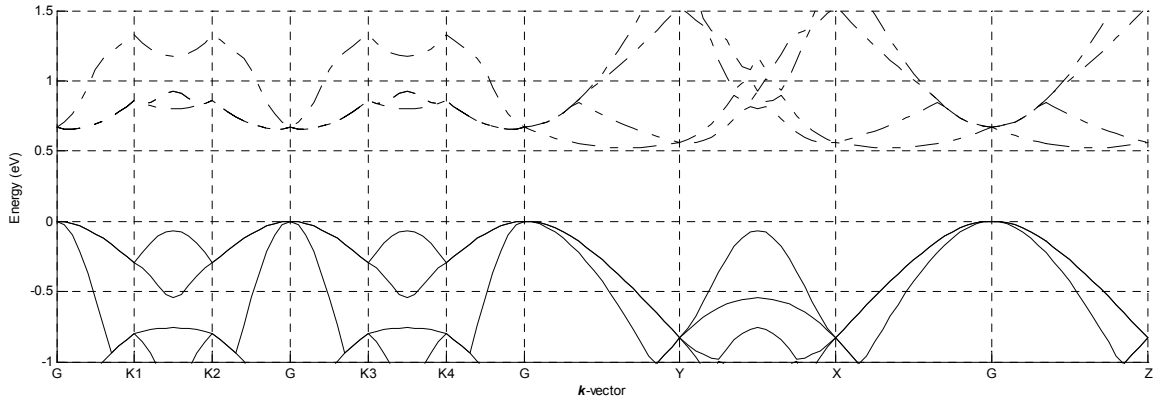

Fig. 4 c-Si band structure. G, K1, K2, K3, K4, X, Y and Z corresponds to *k*-points (0,0,0), (¼,¼,¼), (-¼,¼,¼), (-¼,-¼,¼), (¼,-¼,¼), (½,0,0), (0,½,0) and (0,0,½) respectively.

2.2 Self-Interstitial

The diffusion of impurity atoms in silicon is highly influenced by intrinsic defects such as self-interstitials and vacancies. In particular Si self-interstitial is known to enhance the B diffusion (Windl *et al.*, 1999). Therefore it is of great importance to improve our understanding of the behavior of these defects.

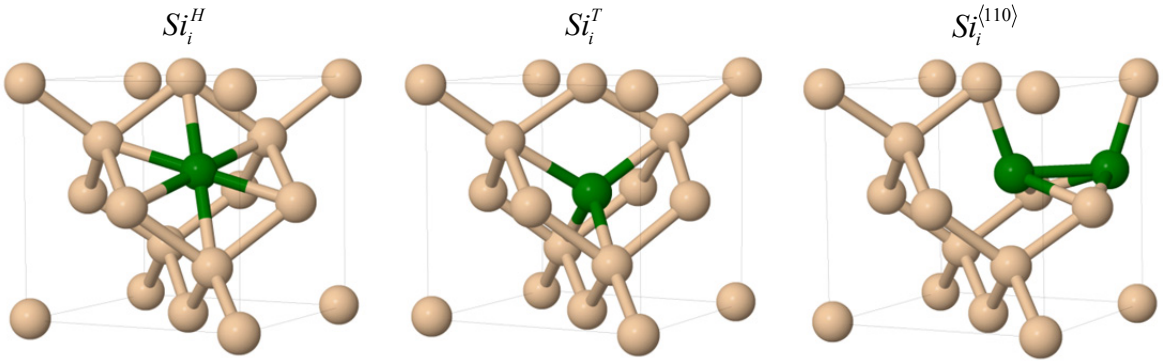

Fig. 5 Common self-interstitial configurations: hexagonal configuration (Si_i^H), tetrahedral configuration (Si_i^T) and split-<110> interstitial. Interstitial silicon atoms highlighted in green.

The silicon self-interstitial configurations that gather more consensus are shown in figure 5. Others less understood configurations, but more energetic, like the "caged" interstitial (Clark and Ackland, 1996, Jones *et al.*, 2008) was not subject of study. The hexagonal interstitial (Si_i^H) is 6-fold coordinated with bonds of length 2.37 Å joining it to six neighbors, which are therefore 5-fold coordinated. The tetrahedral interstitial (Si_i^T) is 4-fold coordinated and has bonds with 2.44 Å of length. It is bonded to its four neighbors, which are therefore 5-fold coordinated. In the split-<110> interstitial ($Si_i^{<110>}$) the two atoms forming the defect are 4-fold coordinated, but two of the surround atoms are 5-fold coordinated. This common dominator from all interstitial defects, which is that the neighbors atoms of interstitial defects are 5-fold coordinated will help identifying these defects in the amorphous samples where apparent order cannot be found.

The formation energy for the self-interstitial defect in silicon may be calculated using the following equation (directly obtained from equation (1.47)),

$$E_f\left(Si_i\right) = E_T\left(Si_{65}\right) - \frac{65}{64} E_T\left(Si_{64}\right). \tag{2.2}$$

The results are presented in Table 2. We found out that the split-<110> interstitial have the lowest formation energy amongst all studied defects, in agreement with the findings from several authors (Zhu *et al.*, 1996; Leung *et al.*, 1999; Jones *et al.*, 2009).

Table 2 Formation energies for all studied interstitial configurations compared to previous *ab initio* studies. Kong (2008) used 64-atom supercells and Leung *et al.* (1999) 32-atom supercells. All quantities are in eV.

configuration	calculated	Kong (2008)	Leung *et al.* (1999)
Si_i^H	3.63	3.87	3.31
Si_i^T	3.77	-	3.43
$Si_i^{\langle 110 \rangle}$	3.51	3.90	3.31

An undesired effect can occur when the <110>-split interstitial is simulated in smaller supercells (64 atoms or lower). Since the <110>-split interstitial creates larger stress field in its neighboring Si lattice, in comparison to the others interstitial configurations, which may not be able to *relax* fully at a smaller supercell (Zhu *et al.,* 1996). This may explain why Kong (2008) obtained lower formation energy for the hexagonal interstitial configuration.

2.3 Boron related point defects

2.3.1 Substitutional Boron

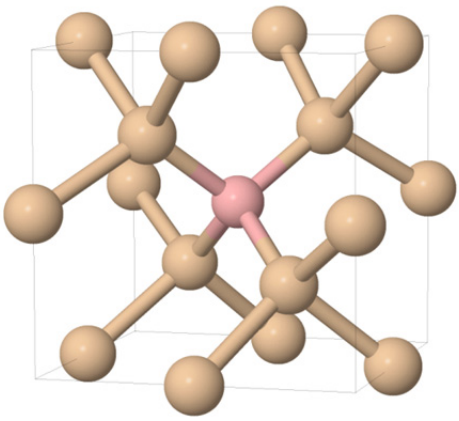

Fig. 6 Substitutional boron configuration. B atom in pink.

Under equilibrium conditions and the limit of low B concentration, B atoms occupy substitutional sites in a c-Si lattice (figure 6). As expected, since the B atom has a smaller atomic radius than the Si atom, the first-nearest-neighbor Si atoms *relax* towards the substitutional B atom by about 12%.

The local vibrational mode where calculated for substitutional boron (B_s). The ^{10}B mode is at 633 cm^{-1} and ^{11}B at 610 cm^{-1}, with an isotopic deviation of 23 cm^{-1}. These modes show good

agreement with experiment (Smith and Angress, 1963): 646 cm^{-1} and 623 cm^{-1}, respectively, and in excellent agreement for the isotopic shift.

The band structure of this defect was also calculated in the same way as in the bulk. The half occupied level is marked in red in figure 7.

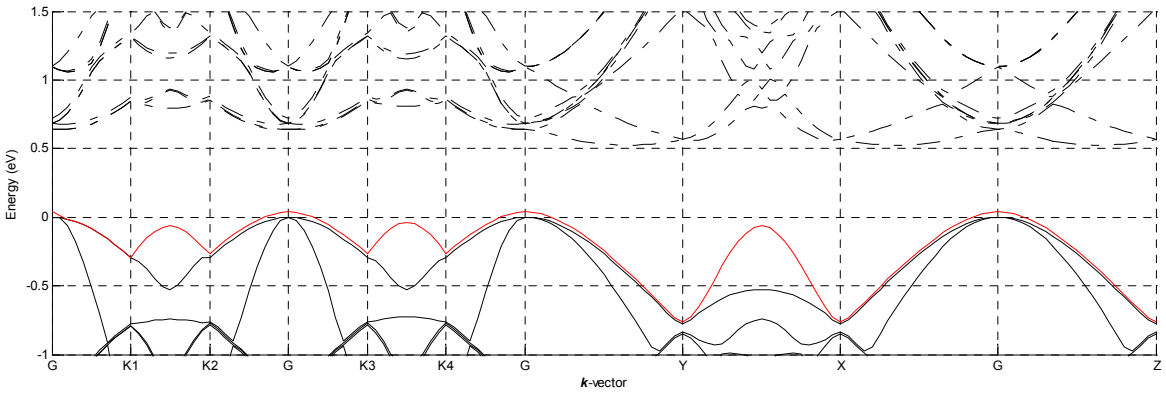

Fig. 7 Band structure for substitutional boron. In the neutral charge state the black lines represent filed levels, the dashed lines represent empty levels and the red line is a half occupied level. G, K1, K2, K3, K4, X, Y and Z corresponds to *k*-points (0,0,0), (¼,¼,¼), (-¼,¼,¼), (-¼,-¼,¼), (¼,-¼,¼), (½,0,0), (0,½,0) and (0,0,½) respectively.

Using gallium as the marker species in the marker method (Coutinho *et al.*, 2002) the (-/0) electric level for substitutional boron was placed at $32\ meV$ above valence band. Experimental technique (Madelung, 1996) placed the same level at $45\ meV$.

2.3.2 Interstitial Boron

A similar approach to model the Si self-interstitial was taken in order to model the interstitial boron. The same interstitial configurations (tetrahedral, hexagonal and split-<110> interstitials) were tested in the neutral charged state by replacing the previous Si interstitial with a B atom.

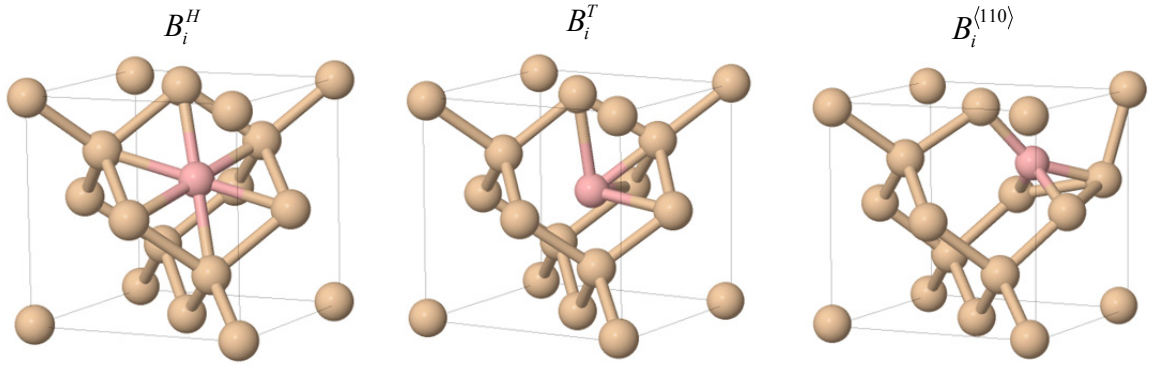

Fig. 8 Common interstitial configurations: hexagonal configuration (B_i^H), tetrahedral configuration (B_i^T) and split-<110> interstitial. Interstitial boron atoms highlighted in pink.

The hexagonal (B_i^H) retained similar structural features from the self-interstitial configuration. The tetrahedral (B_i^T) configuration *relaxed* towards an atom from the lattice, making a smaller bond (2.05 Å) than the remaining 3 neighbours (2.45 Å). Regarding the <110>-split, the minimum energy structure has a small distortion due to the B-Si bond lengths becoming slightly shorter (1.95 to 2.1 Å) than the Si-Si bonds.

The binding energy of the tetrahedral defect is $0.28\ eV$, in good agreement with the interval of 0.2-$0.3\ eV$ established by Hakala *et al.* (2000).

The formation energies for this configuration were determined to be 0.46, 0.48 and $0.48\ eV$ for the B_i^H, B_i^T and $B_i^{\langle 110 \rangle}$, in general lower than the ones by the previous study, which indicates 0.58 and $0.98\ eV$ for the hexagonal and tetrahedral configurations.

2.3.3 Substitutional Boron – Silicon Interstitial

According to Hakala *et al.* (2000) all these interstitial configurations (B_i^H, B_i^T and $B_i^{\langle 110 \rangle}$) are meta-stable and have formation energies between 0.24 to $1.34\ eV$ greater than configurations with boron in a substitutional site bonded to a silicon interstitial ($B_s - Si_i$). We modeled this defect in the same tetrahedral, hexagonal and split-<110> configurations. Regarding the $B_s - Si_i^H$, the structural *relaxation* resulted in the $B_s - Si_i^T$ configuration. Our results are in agreement with Hakala *et al.* (2000) findings, being the difference of the formation energy for the tetrahedral configurations B_i^T and $B_s - Si_i^T$ equal to $0.90\ eV$ and the difference for the $B_i^{\langle 110 \rangle}$ and $B_s - Si_i^T$ equal to $0.15\ eV$.

Chapter III
Boron Defects in Amorphous Silicon

3.1 *Supercells generation and characterization*

Throughout the years, many attempts have been made to model the structure of a-Si, but this earlier models suffered from some drawbacks. One of the earliest models, Polk (1971) and Polk and Boudreaux (1973) seemed satisfactory in its main features, mainly its concordance with experimental data for the radial distribution function (RDF) of a-Si (Moss and Graczyle, 1969). But since this method was cluster based, it suffered from the awkward problems posed by free surfaces. It was a hand-built model so it also suffered from the bias inherent of this build procedure. The model from Henderson (1974) was also a hand-build model but eliminated the surface problems by including periodic boundary conditions. Guttman (1981) has devised a method with periodic boundary conditions but for relatively large supercells (over 200 atoms) the obtained RDF was not in good agreement with experimental data.

The Wooten-Winer-Weaire mechanism (also known as WWW bond-switching) (Wooten *et al.*, 1985) addresses the previous issues with a simple solution. The model starts from a diamond structure with periodic boundary conditions build in from start. Then the structure is repeatedly rearrange by the process illustrated in figure 9, in which tetrahedral bonding is preserved. If enough random rearrangements of this kind are performed, a random-network structure is produced and all identifiable features of the diamond cubic structure will disappear.

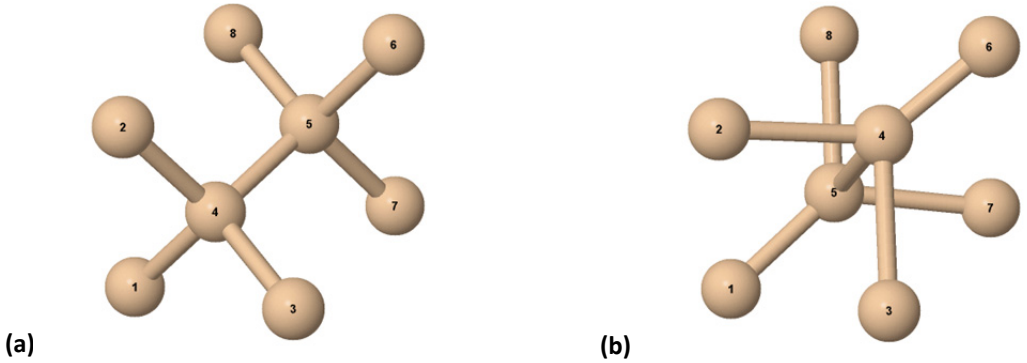

Fig. 9 Local rearrangement of bonds used by the WWW model to generate random networks from the diamond cubic structure. **(a)** Configuration of bonds in the diamond cubic structure. **(b)** *Relaxed* configuration of atoms for a single pair defect.

The WWW bond-switching produces structures of any size with good agreement with experimental data. That has been some adaptations of the WWW mechanism over the years, some in order to prevent the creation of dangling and floating bonds which produce an amorphous solid with a band gap (Santos *et al.*, 2010).

This approach was not chosen in the creation of the following a-Si supercells. Ribeiro *et al.* (2010) performed 15 random bond-switching to the structure in figure 3. Overall 15 different 64-atom samples were made this way and were allowed to *relax* thru the AIMPRO code. These are same supercells used in the following studies and they are represented in the picture below.

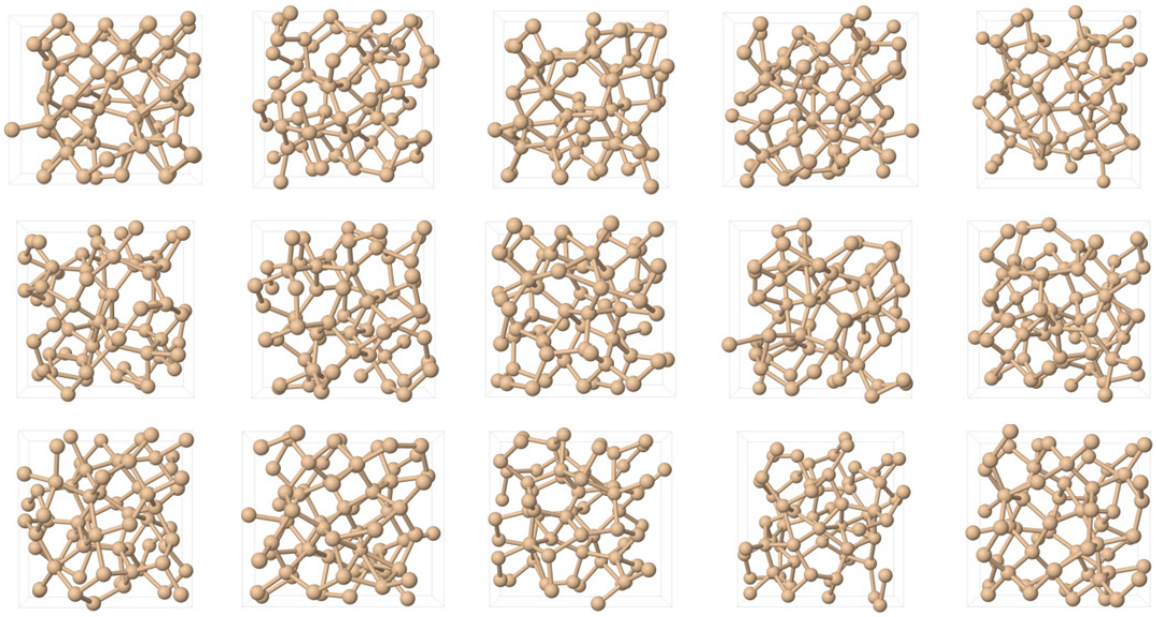

Fig. 10 All 15 amorphous silicon supercells produced by Ribeiro *et al.* (2010) and the same ones used in the following simulations.

The calculated 0.987 density ratio is in good agreement with experimental ratio of 0.982 (Custer *et al.*, 1994). The determined radial distribution (figure 11) is in agreement with experimental data. In the first case, it has the first peak at $0.230\ nm$, close to the experimental value of $0.234\ nm$ (Kugler *et al.*, 1989). The first local minimum in the figure ($0.275\ nm$) established the bond length cut-off. This parameter is important to the atomic coordination study. As we can see in table 3, the majority of atoms have 4-fold coordination, but 3- and 5-fold coordination atoms are also present in different amount across all samples. In these samples, the number of floating bonds is far more superior to the number of dangling bonds, with according to Stutzmann and Biegelsen (1988) is unrealistic and explain the large difference between the total energy (E_T) of each amorphous cell, compared to the total energy of the c-Si cell (E_C).

Table 3 Topological characterization of the 15 cubic supercells of a-Si. E_T-E_C is the difference in total energy of the amorphous cell in comparison to the crystalline one. a_0 is the lattice parameter of the cubic supercell, N_i the number of atoms *i*-fold coordinated and R_n are the number of *n*-atom rings in the sample (same data in Ribeiro *et al.*, 2010).

cell	E_T-E_C (eV)	a_o (nm)	N_3	N_4	N_5	R_4	R_5	R_6	R_7
crystal	0.000	0.53946	0	64	0	0	0	128	0
1	15.814	0.53505	1	58	5	5	25	78	204
2	20.160	0.53904	0	62	2	10	22	63	201
3	19.269	0.53947	0	60	4	8	23	83	194
4	15.919	0.53606	1	58	5	7	24	73	210
5	18.691	0.53903	3	56	5	4	30	75	199
6	21.119	0.53176	0	54	10	13	29	89	247
7	19.047	0.53706	1	54	9	16	23	76	251
8	17.020	0.53684	1	58	5	6	32	64	217
9	19.189	0.53523	2	56	6	7	33	78	194
10	16.919	0.53596	0	56	8	8	36	76	240
11	18.793	0.53812	0	58	6	5	31	79	212
12	20.487	0.53449	2	50	12	12	30	91	257
13	17.554	0.53893	2	62	0	4	29	55	168
14	16.238	0.53746	1	58	5	9	35	72	197
15	13.678	0.53724	0	60	4	3	29	77	213

This difference between total energies can be greater as $21\ eV$ for sample #6, which in this case equals to a $0.33\ eV$ per atom contribution for this increment in energy. In comparison, a_0 does not suffer from great deviation determined for c-Si in section 2.1.

The peak at $109.4°$ in the bond angle distribution (figure 12) is in excellent agreement with the experiment (Laaziri *et al.*, 1999). However while the amorphous supercells show the bond-angle spread across $20°$, in the experimental data this not exceeds $10°$.

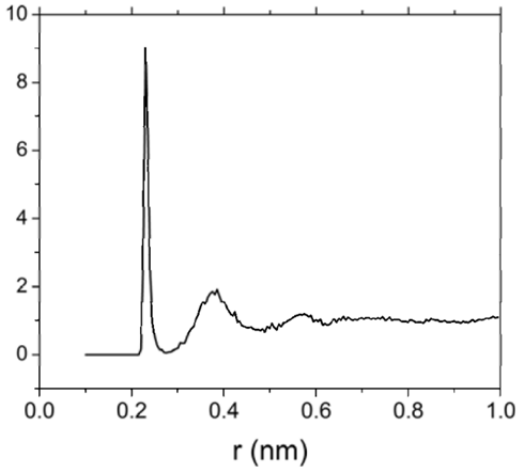

Fig. 11 The radial distribution function for all 15 amorphous cell (Ribeiro *et al.*, 2010).

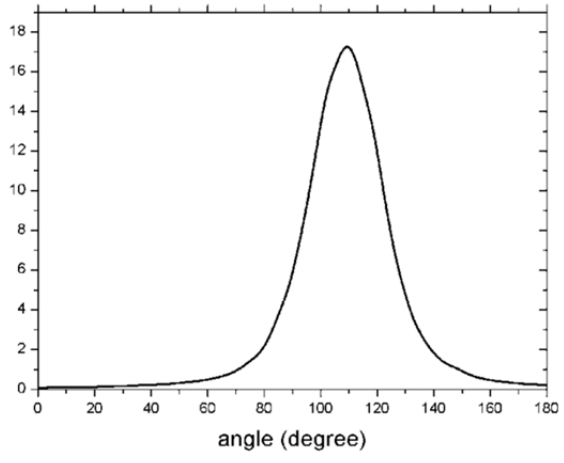

Fig. 12 The bond angle distribution function averaged over 15 samples (Ribeiro *et al.*, 2010).

3.2 Self-Interstitial

In Molecular Dynamics studies (Kong, 2009), a silicon atom is seen to diffuse, while the rest of the amorphous lattice keeps "underformable". With this fact in mind, a silicon self-interstitial can be model as an additional atom in the same volume of the supercell, in which its bonded first neighbors are 5-fold coordinated. We model this defect by choosing several random sites throughout all the 15 samples. The tetrahedral interstitial (Si_i^T) was modeled by placing the additional atom along the direction of a random chosen Si-Si bond. The hexagonal configuration (Si_i^H) was modeled by placing the additional Si atom in the center of a 6-membered ring. Before structural *relaxation* we verified that the majority of atoms that bonded with the interstitial defect became 5-fold coordinated. There were tested 110 different sites across all samples (about 40 different Si_i^H and the remain sites as Si_i^T). The resulted formation energies are presented in table 4.

Table 4 Representative formation energy of the defect when the additional atom was initially at a hexagonal site (E_F [I^H]) and when was initially at a tetrahedral site (E_F [I^T]) are also presented.

cell	E_T-E_C (eV)	E_F [I^H] (eV)	E_F [I^T] (eV)
1	15.814	+0.303	-0.502
2	20.160	-1.494	-1.111
3	19.269	+0.664	-0.400
4	15.919	-0.949	-0.962
5	18.691	-0.934	-1.479
6	21.119	-0.268	-0.324
7	19.047	+0.828	-0.782
8	17.020	+0.774	-0.301
9	19.189	-0.422	-0.382
10	16.919	-0.175	+0.464
11	18.793	-0.031	-0.873
12	20.487	-	-3.364
13	17.554	-0.829	-0.084
14	16.238	+0.756	+1.169
15	13.678	+0.214	+0.734

The correlation between the average formation energy for each sample and the corresponding difference in total energy, regarding the crystalline sample, was tested resulting in a Pearson product-moment correlation coefficient (also known as Pearson's *r*) of -0.4 between the two variables. Appling the guidelines of Cohen (1988) this correlation indicate a medium linear dependence between these observables, hence the greater E_T -E_C became there is a tendency that the smaller (or more negative) will be the formation energy.

In 65 structural *relaxations* (about 60% of the total runs) a widespread structural *relaxation* was observed when the additional Si atom was put in place. And these structural *relaxations* resulted in the majority of negative formation energy with lead us to believe that in these cases the silicon self-interstitial was not successfully simulated. We believe that the resulting structures are in fact new samples with 65 silicon atoms within the same volume as the ones with 64-atom samples. The structural rearrangement across all structure of each individual sample in order to accommodate the additional silicon atom in a 4-fold coordination, as well as its neighbors, further strengths this theory. The resulting new sample has a lower total energy than the original one, even with an additional atom.

Table 5 Formation energies for the self-interstitials in the lowest total energy supercells.

cell	E_T-E_C (eV)			*initially at* I^H	*initially at* I^T
		Si_i final coordination	*configurations*	E_F	E_F
1	15.814	3-	2	+0.972	+0.753
		4-	6	-0.834	-0.874
		5-	2	+0.771	+0.142
4	15.919	3-	1	+0.517	-
		4-	9	-1.315	-0.962
		5-	0	-	-
10	16.919	3-	2	+0.757	+0.994
		4-	2	-1.108	-0.423
		5-	2	-	+0.645
14	16.238	3-	2	+1.041	-
		4-	2	+0.043	-
		5-	2	+1.609	+1.169
15	13.678	3-	1	+0.424	-
		4-	2	-0.305	-
		5-	3	+1.044	+0.734

In an attempt to find real self-interstitials we directed our analysis to the less energetic a-Si supercells, expecting a small atomic overall relaxation (table 5). We obtained a few configurations where the amorphous lattice does not go a great relaxation (like the configuration in figure 13), but this point needs quantitative criteria to be developed.

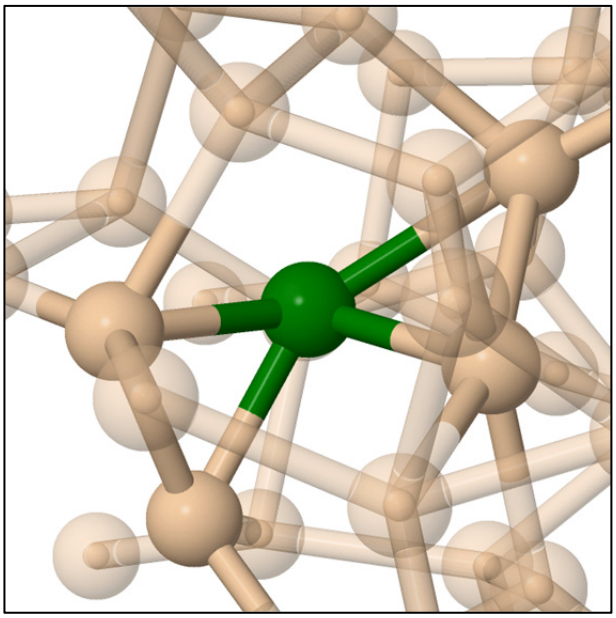

Fig. 13 A representative self-interstitial configuration for a low energetic a-Si supercell. Interstitial silicon atom highlighted in green.

3.3 Boron related point defects

3.3.1 Substitutional Boron

For the substitutional boron defect in the amorphous samples, different approaches were applied. First, for every a-Si supercell a random Si atom was replaced by a B atom. When available, a 3-, 4- and 5-fold coordination Si atoms were picked to be replaced by a B atom and the structure were allowed to be *relaxed*. By this we can evaluate the preferred coordination of the boron species. From 43 analysis runs, roughly 1/3 for each initial atomic coordination for B atom, after structure *relaxation*, we found out that the B atom prefers to have 4-fold coordination as shown in table 6. In most simulations were the B atom was placed in the site of a 3- or 5-fold coordinated Si atom, a structural rearrangement occurred in order to accommodate the B atom in a site, not far from the initial one (less than a half-bond length away), but in a way that the B atom became preferable 4-fold coordinated. Contrarily to the case of self-interstitial modeling, this rearrangement is localized and not widespread.

Table 6 Percentage of substitutional B atoms with *i*-fold atomic coordination after successful *relaxation*.

final coordination		
3-fold	*4-fold*	*5-fold*
17%	72%	11%

These results are in agreement with the preferred atomic coordination of B atom in a crystalline medium and in contradiction to what may be expected since boron has only 3 valence electrons.

Since, in the majority of the structural *relaxations*, the B atom has 4-fold coordination, it is expected that they provide each sample with one hole. However, boron doped a-Si has very low efficiency (Stutzmann *et al.*, 1987). Santos *et al.* (2010) proposed recently that this low efficiency is intrinsic to the deformed a-Si lattice, being the hole trapped in distorted-angles regions. We undergo several simulations across all 15 samples and we did find the same intrinsic low acceptor efficiency in our samples.

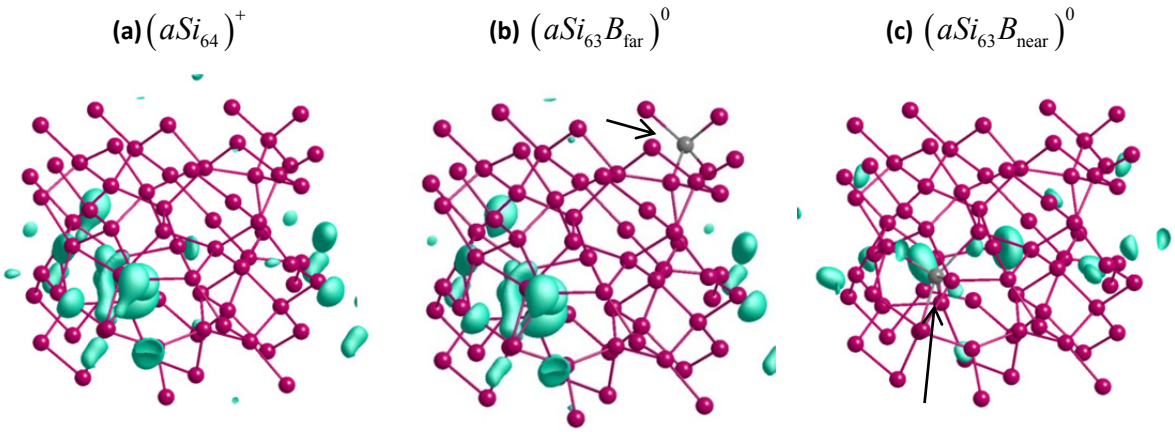

Fig. 14 (a) Localized trapping states in an amorphous a-Si sample. Effect over the localized trapping states by the substitutional boron defect (in grey) if the defect is far from the hole-trap region **(b)** and if the defect is close in the hole-trap region **(c)**.

In the case of an ideal acceptor in c-Si, the hole would be in a shallow state locally extended around the dopant (Wang, 2009). However this did not happen in our simulations as well as in the simulations by Santos *et al.* (2010). In figure 14 we represent the hole location for different B configurations. For the configuration shown in figure 14 (b) the hole is far from the B atom. In fact that the hole location is independently of the B position. When the B atom is near of the hole location [figure 14 (c)] the hole-localization is even stronger.

To determine whether the hole-localization region is induced by the B atoms or it exists even in the absence of acceptors, we analyzed an undoped 64-atom amorphous cell with positive charge $(aSi_{64})^{+}$ [figure 14 (a)], i.e., with the same number of electron than the neutral B configuration $(aSi_{63}B)^{0}$. The resulting hole-localization is very similar to that of figure 14 (b). Therefore, the region of interest is not induced by the B atoms but is inherent to the a-Si matrix.

Its origin is not yet quite understood, but that have been some theories: Pan *et al.* (2008) suggests that this hole traps occurs in regions were the bond lengths are slightly smaller than the overall bond length in the supercell; Both calculations by Bagolini *et al.* (2009) and Wagner and Grossman (2008) attribute this highly localized trapping states to distorted small bond angles. In our samples both previous characteristics occurs in the hole-trap region, were an average bond angle of $\sim 80°$ was observed and slightly small bonds (smaller by ~ 0.2 Å).

We have calculated the local frequencies (LVM) for 4-fold coordinated boron. Relatively to the c-Si the LVM's are higher, up to 840.19 cm^{-1}, and are spread by 250 cm^{-1}. The isotopic LVM shift from ^{10}B to ^{11}B are in average 28 cm^{-1}, 27% higher than the correspondent crystalline isotopic shift.

3.3.2 Boron – Silicon pair

Keeping in mind the findings from the boron-silicon complexes in crystalline silicon (sections 2.3.2 and 2.3.3), to model the boron-silicon pair we started with a random substitutional site in the amorphous sample and replaced with a B atom (atom #6 in figure 15). An interstitial silicon atom was placed in the vicinity of the picked substitutional site (atom #12). The majority of its neighbors became 5-fold coordinated.

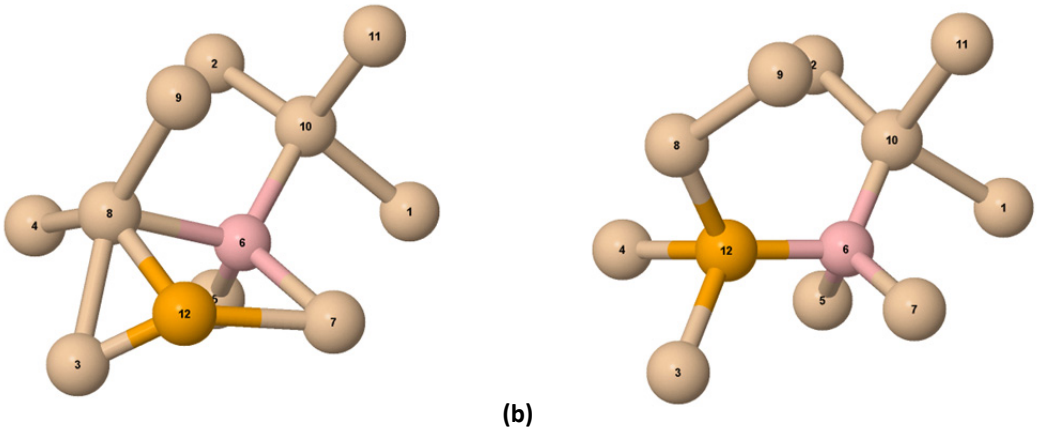

(a) **(b)**

Fig. 15 (a) Initial and **(b)** final *relaxed* structure of the boron-silicon pair simulations.

During structure *relaxation*, the interstitial atom kicked-out a silicon atom (atom #8 in figure 14) and occupied its substitutional site.

The majority of all atoms involved became once again 4-fold coordinated as happened in the self-interstitial modeling, including the atom #8. In some runs, the kicked-out atom did not become 4-fold coordinated but 3-fold instead (less than 10% of the runs). A particular run was used in figure 15 to describe our findings, but this kind of *relaxation* and final structure were

observed in all 100 *relaxations* runs, whatever was the initial silicon interstitial position, regarding to the substitutional atom. In the final structure the bond length between the B atom and the Si interstitial was smaller than the others B-Si bonds (no more than 2 Å).

The interstitial boron defect was also tested by placing an additional boron atom in the amorphous samples, throughout 75 different simulations. As observed in the modeling of the self-interstitial, a widespread structural rearrangement throughout all samples also did occur in this case. The final result of all structural *relaxations* performed by the code was always an atom disposition similar of figure 15 (b). In these runs was not uncommon a final 5-fold coordination to the B atom, but the 4-fold coordination was the majority (80%).

Chapter IV
Final Remarks

4.1. Conclusions

We have studied the boron and boron self-interstitial in crystalline and amorphous Si using the density functional theory – pseudopotential code (AIMPRO).

All relevant structural and electronic properties of c-Si were determined. The lattice constant and his corresponding bulk modulus (as well as its first derivative over pressure) were in agreement with experimental data.

The crystalline silicon modeling resulted in excellent results also in agreement with experimental data. The lowest formation energy was calculated for the <110>-split interstitial. This finding is in line with Zhu *et al.,* 1996.

Besides structural optimization, for the substitutional boron, its local vibrational modes were calculated at $633\ cm^{-1}$ and $610\ cm^{-1}$, for ^{10}B and ^{11}B isotopes respectively. These findings are in good agreement with experiments ($646\ cm^{-1}$ and $623\ cm^{-1}$, respectively), which indicate the same isotopic deviation of $23\ cm^{-1}$. The (-/0) electrical level was determined, using gallium as a marker, to be $32\ meV$, a better result from the previous study (Oliveira, 2008) but still denoting some underestimation of the experimental $45\ meV$ value.

During the modeling of the interstitial boron defect we denote a small structural distortion, as expected since the B atom has a smaller atomic radius. The binding energy of the tetrahedral defect was obtained within the experimental interval previously reported ($0.28\ eV$ within the 0.2 to $0.3\ eV$ experimental value). The calculated formation energies were all underestimated in comparison with Hakala *et al.* (2000) but we did confirmed that interstitial boron configurations are energetically less favorable than $B_s - Si_i$ defects.

Amorphous Si studies

We have modeled the self-interstitial, substitutional boron and B-Si complexes in 64 Si atom supercells. We have used 15 amorphous supercells (Ribeiro *et al.*, 2010) that was proven by topological and vibrational characterization that these supercells have features like radial distribution, bond angle distribution, vibrational density of states, Raman spectra and electronic

density of states in accordance with experimental data which lead us to believe that they in fact are good samples for our first modeling studies in this kind of material.

For the silicon self-interstitial defect in a-Si modeling we add a Si atom in several random sites. During the majority of the 100 structural *relaxations*, all interstitial atoms and its corresponding neighbors took 4-fold atomic coordination, enabled by a widespread structural rearrangement that took the code more than 80 iterations to achieve an optimal structure. The average negative formation energy, in conjunction with the widespread structural rearrangements suffered by the samples, leads us to believe that in these particular runs we did not successfully modeled the silicon self-interstitial defect. Instead we get a new kind of 65-atom amorphous samples with the same volume but with a lower total energy than the corresponding 64-atom sample.

During the study of the boron substitutional defect we realize that the B atom prefers a 4-fold atomic coordination. We also confirmed the existence of intrinsic localized hole-traps in our samples. We observed all features that had been indicated as causes for this phenomenon: localized small bonds and distorted angles. We confirm the presence of a substitutional B atom near the vicinity of these traps further enhances its localized effect. These trapping states lower the doping efficiency, which is a major drawback in the practical use of a-Si.

The boron-silicon pair was also modeled and some kind of a kick-out mechanism was observed during structure *relaxation*. In the majority of the computational runs, the Si interstitial atom kicks-out a substitutional atom, occupies its place, but the kicked-out atom will occupy a near non-substitutional site but in a way that its 4-fold atomic coordination prevails as well as the atomic coordination of its neighbors. The interstitial boron defect was also tested throughout 75 runs and the resulting structure was similar to the one from $B_s - Si_i$. These defects requires further understanding.

4.2. Future Work

During our studies in the amorphous samples we encounter some minor irregularities with the structure of the supercells. We notice that atoms #1 and #2 did not significantly change his positions across all samples which may indicate a minor glitch in the WWW algorithm or insufficient number of performed bond switches. Also we notice that, at the borders of the supercells, some crystalline features were visible. Increasing the number of random bond switches to 100 may overcome this situation but nevertheless this finding needs more attention and further study in order to insure the truth amorphisation of the samples. Besides improving

the algorithm for amorphous cells generation, 1000 atoms or even bigger amorphous cells should be generated and studied, taking advantage from the latest and fastest AIMPRO code, which implements a basis functions filtering scheme (Rayson and Briddon, 2009). This will enable a more accurate and wide study of defects in a-Si.

The self-interstitial in a-Si needs a more quantitative analysis. We have to evaluate the overall lattice relaxation to judge if we obtain a real self-interstitial or just a overall lattice relaxation to a lowest metastable configuration.

Further understanding of B complexes in a-Si and its behavior is definitely a subject for future works. It will also be quite interesting seeing these same techniques used in other materials, like amorphous germanium or other amorphous alloys, like SiGe (Edelman *et al.*, 2008).

These same studies might be performed in samples generated with algorithm adaptations from the original WWW mechanism, especially samples with a band gap (Barkema and Mousseau, 2000).

Bibliography

Adey J, Goss J P, Jones R and Briddon P R, Phys. Rev. B **67**, 245325 (2003*a*).

Adey J, Goss J P, Jones R and Briddon P R, Physica B **340-342**, 505 (2003*b*).

Adey J, *Boron Related Point Defects in Silicon* (University of Exeter, Exeter, 2004).

Angress J F, Goodwin A R, Smith S D, Proc. R. Soc. London, Ser. A **287**, 64 (1965).

Bagolini L, Mattoni A and Colombo L, Appl. Phys. Lett. **94**, 053115 (2009).

Baldereshi A, Phys. Rev. B **7**, 5212 (1973).

Balkanski M and Nazarewicz W, J. Phys. Chem. Solids **27**, 671 (1966).

Bang J, Kang J, Lee W-J, Chang K J, Kim, H, Phys. Rev. B **76**, 064118 (2007).

Barkema G T and Mousseau N, Phys. Rev. B **62**, 4985 (2000).

von Barth U and Hedin L, J. Phys. C **5**, 1629 (1972).

Bean A R, Morrison S R, Newman R C, Smith R S, J. Phys. C **5**, 379 (1972).

Beattie A G and Schirber J E, Phys. Rev. B **1**, 1548 (1970).

Birch F, Phys. Rev. **71**, 809 (1947).

Born M and Huang K, *Dynamical Theory of Crystal Lattices* (Oxford University Press, Oxford, 1954).

Born M and Oppenheimer R, Ann. Physik **84**, 457 (1927).

Brenner D W, Dunlap B I, Harrison J A, Mintmire J W, Mowrey R C, Robertson D H and White C T, Phys. Rev. B **44**, 3479 (1991).

Brust D, *Methods in Computational Physics* **8**, 33 (Academic Press, New York, 1968).

Ceperley D M, Phys. Rev. B **18**, 3126 (1978).

Ceperley D M and Alder B J, Phys. Rev. Lett. **45**, 566 (1980).

Chadi D J and Cohen M L, Phys. Rev. B **7**, 692 (1973).

Chelikowsky J R and Cohen M L, Phys. Rev. B **14**, 556 (1976).

Clark S J and Ackland G J, Phys. Rev. B **56**, 47 (1997).

Cohen J, *Statistical power analysis for the behavioral sciences* (Lawrence Erlbaum Associates, New York, 1988).

Coutinho J, *Oxygen-related Point Defects in Silicon and Germanium* (University of Exeter, Exeter 2001).

Coutinho J, Jones R, Briddon P R, Öberg S, Murin L I, Markevich V P, Lindstörm J L, Phys. Rev. B **65**, 014109 (2002).

Cowern NEB, Zalm PC, van der Sluis P, Gravesteijn D J, de Boer WB, Phys. Rev. Lett. 72, 2585 (1994).

Custer J S, Thompson M O, Jacobson D C, Poate J M, Roorda S, Sinke W C and Spaepen F, Appl. Phys. Lett. **64**, 437 (1994).

Doren V V, Alsenoy C V and Geerlings P, *Density functional theory and its application to materials* **577** (IoP Institute of Physics Publishing Ltd, New York, 2001).

Edelman L A, Phen M S, Jones K S, Elliman R G and Rubin L M, App. Phys. Lett. **92**, 172108 (2008).

Ewald P P, Ann. Physik **64**, 253 (1921).

Fahey P M, Griffin P B, Plummer J D, Rev. Mod. Phys. **61**, 289 (1989).

Feynman R P, Phys. Rev. **56**, 340 (1939).

Fock V, Z. Phys. A **61**, 126 (1930).

Flynn C P, *Point defects and diffusion* (Oxford University Press, Glasgow, 1972).

Guttman L, Phys. Rev. **B** 23, 1866 (1981).

Hakala M, Puska M J and Nieminen R M, Phys. Rev. B **61**, 8155 (2000).

Hartwigsen C, Goedecker S, Hutter J, Phys. Rev. B **58**, 3641 (1998).

Harrison W A, *Pseudopotentials in the theory of metals* (W. A. Benjamin, New York, 1966).

Heine V, Solid State Phenomena **24**, I (1970).

Hellmann H*, Einführung in die Quantenchemie* (Franz Deuticke, Leipzig, 1937).

Henderson D, J. Non-Cryst. Solids **16**, 317 (1974).

Hohenberg P and Kohn W, Phys. Rev. **136**, B864 (1964).

James A M and Lord M P, *Macmillan's Chemical and Physical Data* (Macmillan, London, 1992).

Jeong J W and Oshiyama A, Phys. Rev. B **64**, 235204 (2001).

Jones R and Briddon P R, *Semiconductors and Semimetals*, **51A**, cap. 6 (Academic Press, Boston, 1999).

Jones R, Carvalho A, Goss J P and Briddon P R, Mat. Sc. Eng. B **159-160**, 112 (2008).

Jones R, Goss J, Ewels C, Öberg S, Phys. Rev. B **50**, 8378 (1994).

Jones R O and Gunnarsson O, Rev. Mod. Phys. **61**, 689 (1989).

Kemble, Rev. Mod. Phys. **1**, 206 (1932).

Kohn W and Sham L J, Phys. Rev. **140**, A1133 (1965).

Kong N, Kirichenko T A, Hwang G S and Banerjee S K, Appl. Phys. Lett. **93**, 082109 (2008).

Kong N, *Dopant Behavior in Complex Semiconductor Systems* (University of Texas, Austin, 2009).

Koopmans T, Physica **1**, 104 (1934).

Kugler S, Molnár G, Petö G, Zsoldos E, Rosta L, Menelle A, Belissent R, Phys. Rev. B **40**. 8030 (1989).

Laaziri K, Kycia S, Roorda S, Chicoine M, Robertson J L, Wang J and Moss S C, Phys. Ver. B **60**, 13520 (1999).

Leeuw S W D, Perram J W, R. S E, Proc. R. Soc. London, Ser. A **373**, 27 (1980).

Leung W-K, Needs R J, Rajagopal G, Itoh S and Ihara S, Phys. Rev. Lett. **83**, 2351 (1999).

Lever R F, Bonar J M, Willoughby A F W, J. Appl. Phys. **83**, 1988 (1998).

Louie S G, Froyen S, Cohen M L, Phys. Rev. B **26**, 1738 (1982).

Low J J, Kreider M L, Pulsifer D P, Jones A S and Gilani T H, Am. J. Und. Research **7**, 27 (2008).

Lundqvist S and March N H, *Theory of the inhomogeneous electron gas*, *Physics of solids and liquids* (Plenum, New York, 1983).

Madelung O, editor, *Semiconductors - Basic Data*, (Springer-Verlag, Berlin, 1996).

MacDonald J K L, Phys. Rev. **43**, 830 (1933).

Marques M A and Gross E K U, Anneal. Rev. Phys. Chem. 85, 427 (2004).

Mc Weeney R, *Methods of Molecular Quantum Mechanics* (Academic Press, New York, 1989).

Mirabella S, Salvador D D, Bruno E, Napolitani E, Pecora E F, Boninelli S, Priolo F, Phys. Rev. Lett. **100**, 155901 (2008).

Monkhorst H J and Pack J D, Phys. Rev. B **13**, 5188 (1976).

Moss S C and Graczyle J F, Phys. Rev. Lett. **23**, 1167 (1969).

Murnaghan F D, *Proceedings of the National Academy of Sciences*, **30** (National Academy of Sciences, Washington, 1944).

Oliveira T, *Modelação Ab Initio da Difusão do Boro em Silício* (Universidade de Aveiro, Aveiro 2008).

Pack J D and Monkhorst H J, Phys. Rev. B **16**, 1748 (1977).

Pan Y, Inam F, Zhang M and Drabold D A, Phys. Rev. Lett. **100**, 206403 (2008).

Parr R G and Yang W, *Density-functional Theory of Atoms and Molecules* (Oxford University Press, Oxford, 1989).

Perdew J P, *Electronic Structure of Solids '91* (Akademie Verlag, Berlin, 1991).

Perdew J P, Burke K, Ernzerhof M, Phys. Rev. Lett. **77**, 3865 (1996*a*).

Perdew J P, Burke K, Wang Y, Phys. Rev. B **54**, 16533 (1996*b*).

Perdew J P and Wang Y, Phys. Rev. B **45**, 13244 (1992).

Perdew J P and Zunger A, Phys. Rev. B **23**, 5048 (1981).

Pickett W E, Comp. Phys. Rep. **9**, 115 (1989).

Polk D E , J. Non-Cryst. Solids **5**, 365 (1971).

Polk D E and Boudreaux D S, Phys. Rev. Lett. **31**, 92 (1973).

Rajagopal A K and Callaway J, Phys. Rev. B **7**, 1912 (1973).

Rayson M J and Briddon P R, Phys. Rev. B **80**, 205104 (2009).

Reif F, *Fundamentals of Statistical and Thermal Physics* (McGraw-Hill, New York, 1965).

Ribeiro R M, Torres V J B,Vasilevskiy M I, Barros A, Briddon P R, Phys. Status Solidi C **7**, 1432 (2010).

Roothaan C C J, Rev. Mod. Phys. **23**, 69 (1951).

Runge E and Gross E K U, Phys. Rev. Lett. **52**, 997 (1984).

De Salvador D, Napolitani E, Mirabella S, Bruno E, Impellizzeri G, Bisognin G, Pecora E F, Priolo F, Carnera A, Mater. Sci. Eng. B **154-155**, 240 (2008).

Santos I, Castrillo P, Windl W, Drabold D A, Pelaz L and Marqués L A, Phys. Rev. B **81**, 033203 (2010).

Smith S D and Angress J F, Phys. Lett. **6**, 131 (1963).

Singh J, *Physics of Semiconductors and Their Heterostructures* (McGraw-Hill, New York, 1993).

Slater J C, Phys. Rev. **34**, 1293 (1929).

Slater J C, *Quantum Theory of Molecules and Solids*, **2** (McGraw Hill, New York, 1965).

Stolk P A, Gossmann H J, Eaglesham D J, Poate J M, Nucl. Instrum. Methods B **96**, 187 (1995).

Stoneham A M*, Theory of Defects in Solids* (Oxford University Press, London, 1975).

Stutzmann M, Biegelsen D K and Street R A, Phys. Rev. B **35**, 5666 (1987).

Stutzmann M and Biegelsen D K, Phys. Rev. Lett. **60**, 1682 (1988).

Tao J, Perdew J P, Almeida L M, Fiolhais C, Kümmel S, Phys. Rev. B **77**, 245107 (2008).

Thijssen J M, *Computational Physics* (Cambridge University Press, Cambridge 1999).

Tipping A and Newman R C, Semicond. Sc. Tech. **2**, 389 (1987).

Troxell J R and Watkins G D, Phys. Rev. B **22**, 921 (1980).

Vosko S H, Wilk L, Nusair M, Can. J. Phys. **58**, 1200 (1980).

Wagner L K and Grossman J C, Phys. Rev. Lett. **101**, 265501 (2008).

Wang L-W, J. Appl. Phys. **105**, 123712 (2009).

Windl W, Bunea M M, Stumpf R, Dunham S T, Masquelier M P, Phys. Rev. Lett. **83**, 4345 (1999).

Windl W, Stumpf R, Liu X –Y, Masquelier M P, Comp. Mat. Sc. **21**, 496 (2001).

Wooten F, Winer K, Weaire D, Phys. Rev. Lett. **54**, 13 (1985).

Zallen R, *The Physics of Amorphous Solids* (John Wiley & Sons, Inc., New York, 1983).

Zhu J, Diaz de la Rubia T, Yang L H, Mailhiot C, Gilmer G H, Phys. Rev. B **54**, 4741 (1996).